BNL-108299-2015-JA

Thermoresponsive PNIPAM Coatings on Nanostructured Gratings for Cell Alignment and Release

Mikhail Zhernenkov[†*], *Rana Ashkar*[‡,§*], *Hao Feng*[||], *Olukemi O. Akintewe*[⊥], *Nathan D. Gallant*[¦], *Ryan Toomey*[⊥], *John. F. Ankner*[¶], *and Roger Pynn*[||,#]

[†] National Synchrotron Light Source II, Brookhaven National Laboratory, Upton, NY 11973, USA

[‡] Materials Science and Engineering Department, University of Maryland, College Park, MD 20742, USA

[§] Center for Neutron Research, National Institute of Standards and Technology, Gaithersburg, MD 20899, USA

[||] Center for the Exploration of Energy and Matter and Physics Department, Indiana University, Bloomington, IN 47405 USA

[⊥] Department of Chemical and Biomedical Engineering, University of South Florida, Tampa, FL 33620, USA

[¦] Department of Mechanical Engineering, University of South Florida, Tampa, FL 33620, USA

[¶] Spallation Neutron Source, Oak Ridge National Laboratory, Oak Ridge, TN 37831, USA

[#] Neutron Sciences Directorate, Oak Ridge National Laboratory, Oak Ridge, TN 37831, USA

Abstract

Thermoresponsive poly(N-isopropylacrylamide) (PNIPAM) has been widely used as a surface coating to thermally control the detachment of adsorbed cells without the need for extreme stimuli such as enzyme treatment. Recently, the use of 2D and 3D scaffolds in controlling cell positioning, growth, spreading and migration has been of a great interest in tissue engineering and cell biology. Here, we use a PNIPAM polymer surface coating atop a nanostructured linear diffraction grating to controllably change the surface topography of 2D linear structures using temperature stimuli. Neutron reflectometry and surface diffraction are utilized to examine the conformity of the polymer coating to the grating surface, its hydration profile, and its evolution in response to temperature variations. The results show that, in the collapsed state, the PNIPAM coating conforms to the grating structures and retains a uniform hydration of 63%. In the swollen state, the polymer expands beyond the grating channels and absorbs up to 87% water. Such properties are particularly desirable for 2D cell growth scaffolds with a built-in non-extreme tissue-release mechanism. Indeed, the current system demonstrates advanced performance in the effective alignment of cultured fibroblast cells and the easy release of the cells upon temperature change.

KEYWORDS: PNIPAM coating, thermoresponsive nanostructured scaffolds, cell alignment and release, neutron reflectometry.

INTRODUCTION

Recent advances in tissue engineering have motivated significant progress in polymer chemistry, biophysics and cell biology. Tissue engineering involves combining living cells, biomaterials and engineering methods to repair, replace or restore damaged tissue. The process requires delicate control of the microenvironment of the cells, particularly the scaffold, since its 3-dimensional structure and properties govern the functionality of the grown tissue[1]. 2D structured surfaces and 3D scaffolds are of a great interest in modern tissue engineering due to their nontrivial effect on the elongation and proliferation of the cultured cells[2]. The cell adhesion to such structures has been a focus for biophysical research and cell biology for a long time[3,4,5,6]. However, a detailed and complete understanding of the processes involved is still lacking. It has been shown that the properties and parameters of the cell matrix have a dramatic effect on the grown cells[7], in particular, such scaffold properties as texture, water content, hydrophobicity and rigidity can affect the cell morphogenesis and proliferation[8,9,10]. One of the most important properties of the scaffolds is the ability to controllably release the grown tissue with minimal or no damage to the tissue structure or functionality. For example, sometimes the adhesion of cells to 2D or 3D scaffolds is so strong that the use of potentially toxic enzymes or mechanical force is required in order to harvest cells for further processing. To avoid such potentially harmful influence on the grown tissue different approaches have been proposed, which mostly involve the use of synthetically modified surfaces[11,12].

One of the most promising candidates for controllable release of cultured cell sheets is poly(N-isopropylacrylamide) (PNIPAM) polymer. PNIPAM is non-toxic at physiological temperatures and when temperature is increased above 32°C (the lower critical solution temperature, LCST) it undergoes a structural transition which results in the collapse of the polymer and successful cell

adherence and growth[13]. PNIPAM has been widely used to study and control cell adhesion on flat surfaces including grafted surfaces of PNIPAM monolayers[14,15,16,17,18]. Recently, the possibility of using submicrometer-grooved PNIPAM for constructing aligned cell sheets was explored[19]. Unfortunately, the determination of the PNIPAM properties in a nanostructured geometry remains a challenge under aqueous conditions using conventional microscopy techniques[19].

On the other hand, X-ray and neutron reflectometry techniques have proved to be useful in such nanoscale characterizations and in providing detailed information of the surface topology and in-depth profile of thin coatings[20,21] in dry and fluid environments. In this work, we utilize neutron reflectometry and grazing-incidence neutron surface diffraction to determine the thermal response of nanostructured PNIPAM coatings deposited on a linear diffraction grating with submicron features using a simple standard spin-coating technique. The scattering patterns obtained from the PNIPAM-grating system above and below the transition temperatures accurately determine the changes in the surface structure and water uptake in response to temperature stimuli. These detailed measurements are particularly crucial for the implementation of submicrometer-grooved PNIPAM in constructing aligned cell sheets[19], due to their nontrivial effect on the elongation and proliferation of the cultured cells[2]. In these systems, the cell morphogenesis and proliferation are determined by scaffold properties such as groove topology, surface coverage, and water content[8,9,10] which are investigated here. Also, using a proof-of-principle experiment, we demonstrate the effectiveness of the current scaffold in controlling the orientation and release of fibroblast cells. The results of this study provide insights into such applications as controlling cardiomyocyte orientation on microscaffolds[2] and induced switching of cell adhesion and harvesting[3,4,5,6].

MATERIALS AND METHODS

Materials. PNIPAM polymer was spin-coated on a silicon grating (purchased from LightSmyth technologies) with a nominal pitch and groove-depth of d = 833 nm and h = 250 nm, respectively, which were independently verified with neutron scattering. Before polymer deposition, the Si grating was thoroughly cleaned by alternating rinses of chloroform, toluene, methanol and high purity deionized water. Following the rinse, the grating was placed in an ozone cleaner for 20 min, after which the Si surface was modified with 3-amino-propyltriethoxysilane. Finally, poly(N-isopropylacrylamide) copolymerized with methacroylbenzophenone (PNIPAM-co-MaBP) was spin coated on the Si grating and cross-polymerized using ultraviolet light[22,23] . The PNIPAM–coated Si grating was measured in D_2O by grazing incidence neutron scattering using the solid-liquid interface cell shown in Figure 1. The cell is composed of a thick silicon wafer (shown in the top left corner of Figure 1) and a transparent quartz window (with fluid inlet ports) as the sandwiching blocks and a PDMS gasket as a seal. The entire sample cell was held in place with aluminum clamps, one of which accommodated two resistive heating barrels. More details about the design of the sample cell can be found elsewhere[24].

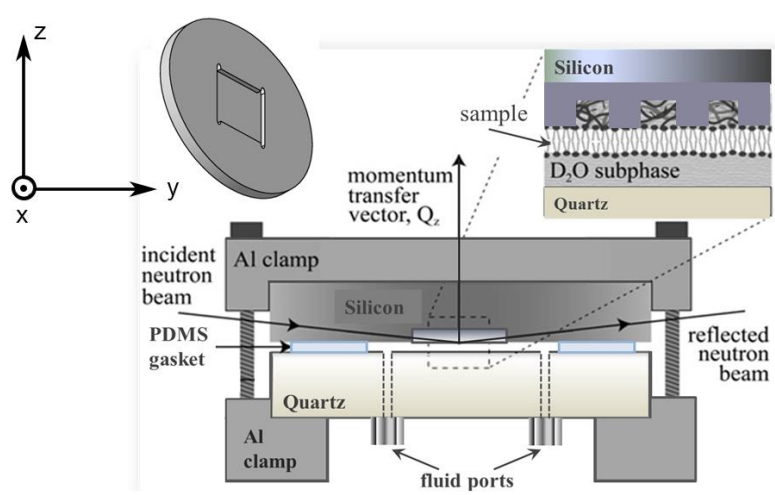

Figure 1. Scheme of the liquid-solid interface cell used for the neutron reflectivity experiment described in the text. The scattering geometry is identified by the Cartesian reference frame where the x- and y-axes are in the plane of the grating along and perpendicular to its lines, respectively, and the z-axis is normal to the average grating surface. The insert at the top left shows the silicon wafer through which the neutron beam is incident on the sample. In the middle of the block is the trench in which the grating is placed during the experiment.

Neutron Scattering Measurements. The neutron reflectometry (NR) experiment was performed at the liquid reflectometer (beamline 4B) at the Spallation Neutron Source at Oak Ridge National Laboratory[25]. Two types of scattering, specular reflection and off-specular Bragg scattering, were recorded. The intensity of the specularly reflected beam is generally measured as a function of the wavevector transfer normal to the sample surface, $Q_z = \frac{4\pi}{\lambda}\sin\theta$, where λ is the neutron wavelength and θ is the incident angle of the neutron beam. This type of measurement probes the depth profile of the sample (with Angstrom resolution[26,27]) averaged over the coherent area of the neutron beam on the sample surface. To analyze specular reflectivity data, the nuclear scattering length density (NSLD) profile of the sample was sliced into a number of layers each with a constant NSLD. Interfacial roughness was accounted for by the Nevot-Croce function[28]. The best least-square fit was obtained using genetic optimization followed by the Levenberg-Marquardt nonlinear least squares method[29].

In order to determine the lateral y-z profile of the sample, off-specular neutron surface diffraction was detected. The periodicity of the grating along the y-axis induces dynamical scattering effects that result in off-specular scattering at discrete angles determined by the Bragg-condition[35], $k_y = k_{0y} + m\mathrm{g}$, where k_{0y} and k_y are the y-components of the incident and scattered wavevectors, respectively, $g = 2\pi/d$ is the smallest reciprocal lattice vector and m is an integer.

Due to the conservation of energy and the translational invariance along the x-direction (i.e. $k_x = k_{0x}$), the z-component of the scattered wavevector is also quantized: $k_z = \sqrt{k_{0z}^2 + k_{0y}^2 - (k_{0y} + mg)^2}$. In the present study, only the first order Bragg ridge had enough statistics above the background level. This type of scattering cannot be adequately analyzed with conventional reflectivity models and a dynamical theory approach had to be implemented for proper data analysis. In this work, we used the dynamical theory (DT) algorithm developed by Ashkar et al.[24,30] , which incorporates a Parratt formalism[31] to account for in-depth variations in the sample. We should mention that the scattering geometry (Figure 1) is such that both the incident and the scattered neutron beams are confined in silicon, which is relatively transparent to neutrons, thus minimizing the length of the neutron trajectory in the deuterated fluid in contact with the grating.

RESULTS AND DISCUSSION

The surface topography of a PNIPAM film coating a nanostructured grating was explored by neutron reflectometry and neutron surface diffraction above and below the lower critical solution temperature of PNIPAM under ambient pressure. The detailed analysis of the film morphology required a full characterization of the underlying substrate (bare grating) prior to the PNIPAM-film deposition. In both cases, measurements were carried out in D_2O instead of H_2O to enhance the neutron scattering contrast between the fluid subphase and the Si grating with its polymer coating (cf. Table 1). Although PNIPAM's phase transition temperature in D_2O is one degree higher (306 K) than in H_2O[32], the temperatures in this study (300 K and 315 K) are far from this critical value. Model fits to the specular reflectivity data, using the fitting routine described in the methods section, yielded the thickness and the average NSLD of each layer, as well as the surface and interfacial roughness. The fitted values obtained for the bare grating and the

PNIPAM-coated grating are reported in Table 1. The composition of each layer can be obtained from the average density values, and is consistent with the schematic depiction of the samples shown in Figure 2.

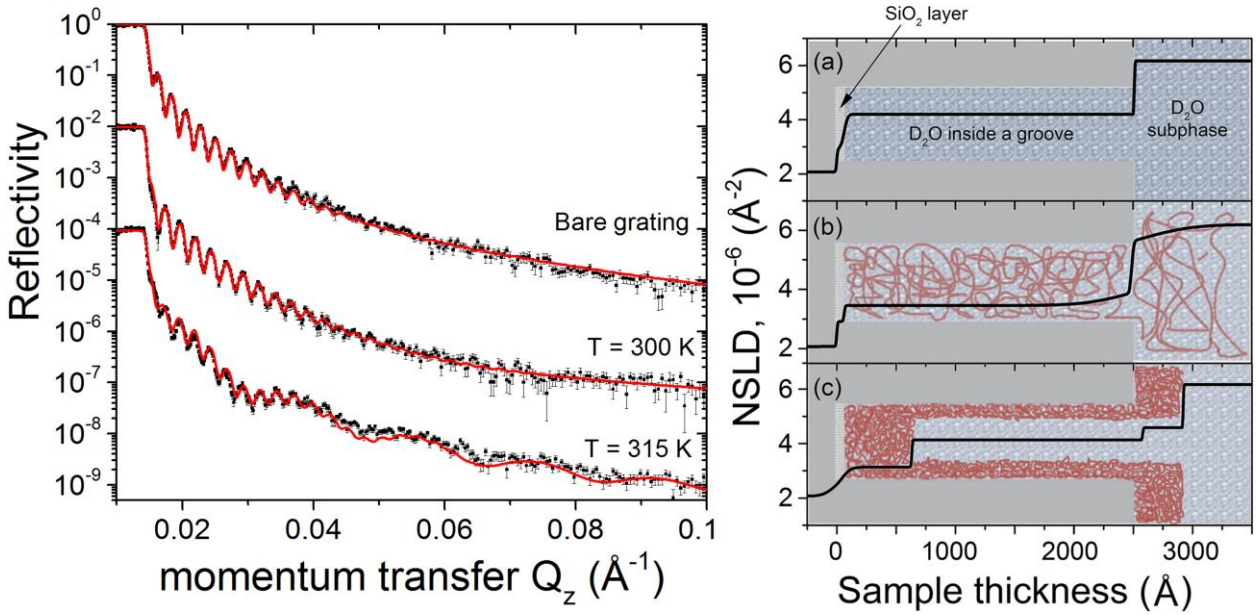

Figure 2. (Left) Specular NR data (black squares) from the bare Si grating and the polymer–coated grating at 300 K and 315 K, along with the fitting curves (solid red lines). The error bars indicate ±1 standard deviation, and the NR curves are offset for clarity. (Right) NSLD profiles (black solid lines) obtained from the NR fits. Also shown (red and blue shading) are schematics of the real space interpretations used to model the experimental data: (a) Bare Si Grating, (b) T = 300 K, (c) T = 315 K. In (b) and (c) PNIPAM polymer is denoted by red entangled lines. In (b), PNIPAM film is fully expanded such that it fills the grating's groove and extends into the D_2O subphase. In (c), the polymer film is in its collapsed state and forms a thin coating on the grating structures (PNIPAM attachment to the walls is determined from Bragg scattering analysis). The thickness of a thin SiO_2 layer at the bottom of the groove was fixed for all 3 models. The grating's pitch-to-depth ratio on the NSLD interpretation is not to scale.

Table 1. Summary of the model parameters obtained from specular reflectivity fits. The model only considers an oxide layer at the bottom of the grooves which is thicker than the normal native oxide layer (about 10 Å) due to the etching conditions involved in lithographic process. The native oxide is expected to be present on the top of the mesas, but is not detectable in the current system.

Bare Si Grating			
Layer	Thickness, Å	NSLD, 10^{-6} Å^{-2}	Roughness, Å
Si grating	--	2.07	
SiO_2+Si	62.0	2.91	7
Si+D_2O	2445.0	4.2	24.4
D_2O subphase	--	6.17	2
T = 300 K			
Si grating	--	2.07	
SiO_2+Si	62.0	2.91	6.1
Si+PNIPAM+D_2O	2425.6	3.46	7.3
PNIPAM+D_2O	63.6	5.19	13.8
D_2O subphase	--	6.17	347.3
T = 315 K			
Si grating	--	2.07	
SiO_2+Si	62.0	2.91	87.3
Si+PNIPAM+D_2O	570.28	3.13	40.6
Si+D_2O	1956.8	4.13	5.3
PNIPAM+D_2O	341.66	4.58	5.2
D_2O subphase	--	6.17	3

The fits to the grating data are consistent with previous microscopic characterization of the grating cross-section, i.e. rectangular profile with groove widths nearly equal to the half-pitch[33]. The NSLD of "Si + D_2O" layer (Table 1, "Bare Si grating") is found to be 4.2×10^{-6} Å^{-2} , which corresponds to about Si (48%)/D_2O (52%) composition. A 62 Å-thick SiO_2 layer was found at the bottom of the grooves. The same grating was used for all measurements presented here (Figure 2), such that the grating parameters obtained from fits on the bare grating are fixed in modeling the PNIPAM depth profile.

For successful fabrication of fine grating scaffolds to control cell orientation, the complete and uniform PNIPAM coverage of the top, bottom, and side walls of the grating must be ensured. At the same time, in order to controllably release and harvest grown tissue from a grating without damage, the tissue release mechanism should provide a complete detachment of the cells from the scaffold. Therefore, to enable tissue release as PNIPAM expands at low temperature, the polymer should preferably completely fill the grooves, which helps expel the cell sheets into the water subphase. Indeed, the fit to the specular reflectivity data taken from PNIPAM on the grating at 300 K demonstrates that at low temperature PNIPAM fills the grating channels and slightly extends into the subphase (by about 700 Å). In Table 1, the NSLD of the "Si+PNIPAM+D_2O" ("T = 300 K" subsection) is 3.46×10^{-6} Å^{-2} which corresponds to 74% uniform PNIPAM hydration in the bottom 2000 Å of the grooves. The hydration of PNIPAM close to the top of the grooves (top 500 Å) gradually increases from 74% to 87% which is evidenced by the upward trend in the NSLD profile between 2000 Å and 2500 Å of the "sample thickness" (Figure 2b).

At T = 315 K the reflectivity curve notably changes (Figure 2, left panel) as compared to the data taken at T = 300 K. The NSLD profile obtained from the fit to the data (Figure 2c) suggests

that, at T = 315 K, PNIPAM is collapsed and forms 570 Å and 341 Å thick polymer layer at the bottom and the top of the grating, respectively. The hydration of the polymer layer at the bottom of the groove is 63%. It is noteworthy, that the hydration of a PNIPAM polymer system strongly depends on the degree of the cross-linking and the specific architecture of the structure. For example, is has been previously reported that asymmetric diblock copolymer Poly(Styrene-b-NIPAM) allows the total water storage of only 17% with a total film thickness increase of as little as 2.5% upon swelling[34]. In the present work, PNIPAM was copolymerized with methacroylbenzophenone (PNIPAM-co-MaBP) and further cross-polymerized using ultraviolet light. The hydration of the polymer both in the collapsed and expanded state is in a good agreement with earlier studies[35]. Similarly, the hydration of about 90% in the swollen state was also reported for the PNIPAM-co-PAA microgels[36,37]. Since the scaffold hydration plays an important role in successful cell growth and harvesting, such dependability of the hydration values on the specific system architecture sets important restrictions on the design of the micro-scaffolds.

It is important to mention, that in order to establish a reproducibility of results, we cycled the temperature twice from 300 K to 315 K and collected specular NR data at each cycle. Comparison of two consecutive cycles between 300 K and 315 K demonstrated excellent reproducibility of the system (data not shown here).

In order to determine whether or not PNIPAM is attached to the side walls of the grating channels, the cross-sectional profile of the PNIPAM coating was extracted from the Bragg scattering using the dynamical theory approach discussed in the methods section. A sample of the Bragg data obtained on the bare and coated grating is shown in Figure 3. The data used for the fits were obtained, after background subtraction, by integrating the scattering intensity over

the whole width of the Bragg ridge for each wavelength. The integrated data with corresponding DT calculations are shown in Figure 3 for the bare grating (Figure 3a) and the polymer-coated grating at 300 K (Figure 3b) and 315 K (Figure 3c).

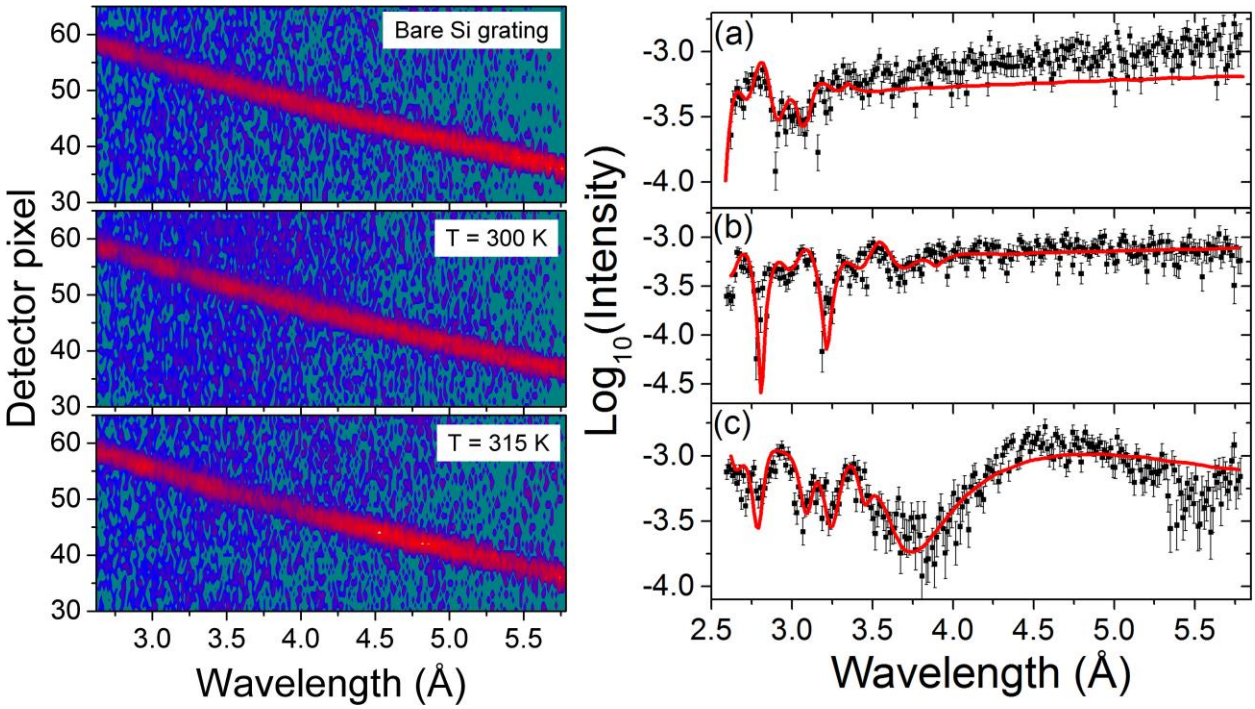

Figure. 3. (Left panel) Detector image showing the 1st order Bragg ridge obtained with the bare grating and with the PNIPAM-coated grating at 300 K and 315 K. (Right panel) Off-specular data integrated over the 1st Bragg ridge as a function of the neutron wavelength for (a) the bare grating and the grating with (b) swollen and (c) collapsed polymer films. The solid red lines represent the DT calculations for a 300 Å thick polymer covering the vertical walls of the grating.

For all Bragg measurements, the incident angle of the neutron beam was 0.15°. The angle between the lines of the grating and the incident beam direction, which is also required for the DT modeling, was set to 90°, which is a good approximation to the experimental settings. The DT model was designed such that, in the case of the bare grating, three layers were considered:

silicon substrate, modulated grating layer and D_2O subphase. For the polymer-coated grating, two additional layers were considered to account for the polymer layers in the bottom of the grooves and on the top of the mesas; the modulated grating layer was modified in the model to account for a polymer layer with variable-thickness on the grating walls. The parameters of the bare grating profile were fixed to the values obtained from the specular data fits. For the polymer-coated grating, NSLD and thickness of the polymer layer at the bottom of the grooves and on top of the mesas were set to the values obtained from the specular data. Consequently, the only fit parameter in the DT calculation was the thickness of the polymer films coating the walls of the grating. The calculation of the Bragg data on the PNIPAM-coated grating at 300 K is consistent with the results obtained from the specular fit. It confirms that, in the swollen state, the PNIPAM film extends beyond the grating mesas. This is an important finding for the implementation of this scaffold in tissue release mechanisms, where a complete detachment and expulsion of the cells from the scaffold is mechanically enabled through the swelling of the polymer beyond the grating channels. In the collapsed state (315 K), the DT calculation shows that a thin PNIPAM layer with the thickness of 300 ± 50 Å coats the vertical walls of the grating. This result is depicted in Figure 2c. The conformity of the polymer to the underlying grating in the collapsed state was independently verified with Atomic Force Microscopy (AFM). The AFM measurements were carried out with Digital Instruments NanoScope atomic force microscope (Santa Barbara, CA). The cantilevers were made of Si, and its resonance frequencies were 150 to 190 kHz. The measurements were performed in tapping mode under ambient air conditions. A 5x5 μm^2 area scan is shown in Figure 4. The micrographs clearly show that the PNIPAM uniformly covers the Si grating and the conformity of the polymer to both sides of the groove is well preserved, in agreement with the neutron reflectometry results.

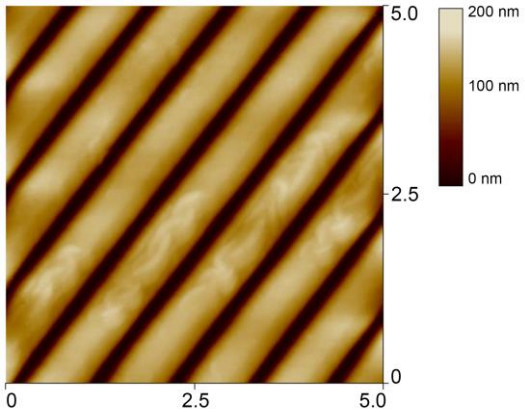

Figure 4. AFM image of the collapsed PNIPAM polymer on the Si grating. The vertical scale is 200 nm.

In order to verify the applicability of PNIPAM coated Si gratings as a surface-tunable micro-scaffold for tissue engineering we performed live cell culture on the system. 3T3 mouse embryonic fibroblast cells were cultured in 10% newborn calf serum (NCS) growth medium containing 1% antibiotics of penicillin and streptomycin stock solution. The cells were then seeded onto the PNIPAM-coated silicon gratings at a density of 110 to 1000 cells/mm^2 and cultured at 37 °C for 24 h (Figure 5a).

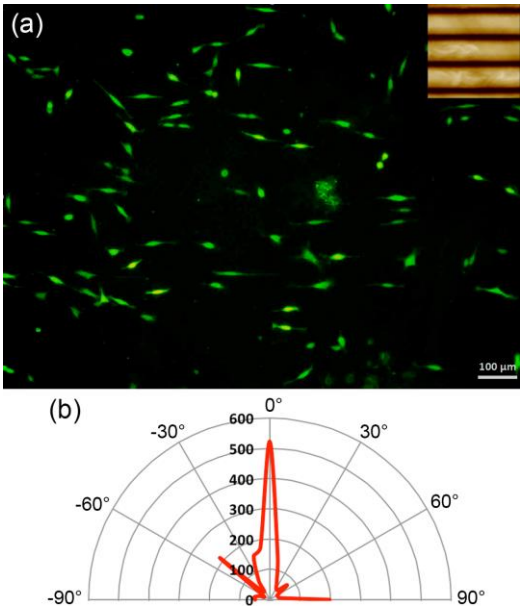

Figure 5. (a) 3T3 mouse embryonic fibroblast cells seeded at the density of the 110 cells/mm^2. The AFM excerpt shown in the insert denotes the grooves direction with the respect to the image. (b) A radial histogram for cell orientation showing primary alignment along 0°, which corresponds to the grooves direction.

Using fluorescent tags, the cells were found to be primarily aligned along the grooves direction of the PPNIPAM scaffold, as demonstrated in the radial histogram shown in Figure 5b. The percent of cells aligned within +/- 10° of the groove direction is 42% and within +/- 20° is 54%, which is in agreement with other studies of cell alignment on nanogratings[38]. Subsequent decrease of the temperature to 4 °C triggered the complete detachment of cells after 90 min.

CONCLUSIONS

Cultured cells on flat PNIPAM substrates are randomly oriented and therefore cannot be used in some specific applications where anisotropic cell alignment is required. In this study, we developed a simple technique that allows grooved PNIPAM surfaces with virtually any geometry to be fabricated and used as tunable substrates with controllable 2D nanostructures. Such control over the surface topography and polymer geometry plays an important role in optimizing the functionality of substrates used in biomaterial scaffold architecture for tissue engineering. Simultaneous analysis of neutron specular reflectivity and off-specular Bragg scattering provided information on the complete 2D structure of the PNIPAM-coated Si grating including the hydration profile of the polymer both in the collapsed and expanded states. These measurements demonstrated that this system maintains a complete and relatively uniform PNIPAM coverage of grating's top, bottom, and side walls and allows for a reproducible switching between collapsed and expanded states. In the collapsed state, the PNIPAM coating conforms to the grating structures and retains a uniform hydration of about 63% whereas in the swollen state, the

polymer expands beyond the grating channels and absorbs up to 87% water. Interestingly, the grating pitch-to-depth ratio is mostly preserved, which is an important requirement for successful fabrication of fine 2D tissue-growth scaffolds to control the cell orientation[2]. Owing to the thermal sensitivity of PNIPAM such a simple structure can be used for cell proliferation and subsequent detachment of intact cell sheets with no damage to the tissue structure or functionality. The applicability of the PNIPAM-coated Si grating as surface-tunable micro-scaffolds was demonstrated using 3T3 mouse embryonic fibroblast cells which were cultured on the scaffold and subsequently detached as an intact cell sheet upon decreasing the temperature beyond the PNIPAM's LCST. The cells clearly exhibited primary orientation along the grooves direction of the PNIPAM-grating scaffold. In summary, we showed that using lithographically structured gratings spin-coated with PNIPAM polymer can provide a powerful yet very simple approach to control the actual groove geometry and possesses a built-in tissue release mechanism, which has been a challenge so far.

AUTHOR INFORMATION

Corresponding Author

*Email: zherne@bnl.gov; rashkar@umd.edu, Tel: +1-631-344-5158

Notes

The authors declare no competing financial interest. Disclaimer: The identification of any commercial product or trade name does not imply endorsement or recommendation by the National Institute of Standards and Technology.

ACKNOWLEDGEMENTS

The authors thank Dr. Candice Halbert for her help in facilitating the use of the chemistry lab and experiment setup at ORNL. Use of the National Synchrotron Light Source-II, Brookhaven National Laboratory, was supported by the U.S. Department of Energy, Office of Science, Office of Basic Energy Sciences, under Contract No. DE-SC00112704. The work at University of South Florida was supported by National Science Foundation DMR-0645574 and CAREER DMR-1056475. O.O.A. was supported by Alfred P. Sloan Foundation Fellowship and UNCF-Merck Dissertation Fellowship. Neutron experiments conducted at ORNL's Spallation Neutron Source was sponsored by the Scientific User Facilities Division, Office of Basic Energy Sciences, US Department of Energy. Oak Ridge National Laboratory is operated by UT-Battelle, LLC under DOE Contract DE-AC05-00OR22725. Work at Indiana University was supported by the US Department of Energy through its Office of Basic Energy Sciences, Division of Material Science and Engineering, grant No. DE-FG02-09ER46279

REFERENCES

1. Bhatia, S. N.; Chen, C. S. Tissue Engineering at the Micro-Scale. *Biomed. Microdevices* **1999**, 2 (2), 131-144.

2. Fujita, A.; Fujita, K.; Nakamura, O.; Matsuda, T.; Kawata, S. Control of Cardiomyocyte Orientation on a Microscaffold Fabricated by Photopolymerization with Laser Beam Interference. *J. Biomed. Opt.* **2006**, 11, 021015.

3. Langer, R.; Vacanti, J. Tissue Engineering. *Science* **1993**, 260, 920-926.

4. Griffith, L. G.; Wu, B. E. N.; Cima, M. J.; Powers, M. J.; Chaignaud, B.; Vacanti, J. P., In vitro Organogenesis of Liver Tissue. *Ann. N.Y. Acad. Sci.* **1997**, 831, 382-397.

5. Ma, P. X.; Zhang, R. Microtubular Architecture of Biodegradable Polymer Scaffolds. *J. Biomed. Mater. Res.* **2001**, 56, 469-477.

6. Ward, J. H.; Bashir, R.; Peppas, N. A. Micropatterning of Biomedical Polymer Surfaces by Novel UV Polymerization Techniques. *J. Biomed. Mater. Res.* **2001**, 56, 351-360.

7. Ratner, B. D.; Bryant, S. J. Biomaterials: Where We Have Been and Where We Are Going. *Annu. Rev. Biomed. Eng.* **2004**, 6, 41-75.

8. Mano, J. F. Stimuli-Responsive Polymeric Systems for Biomedical Applications. *Adv. Eng. Mater.* **2008**, 10, 515-527.

9. Janmey, P. A.; Winer, J. P.; Murray, M. E.; Wen, Q. The Hard Life of Soft Cells. *Cell Motil. Cytoskeleton* **2009**, 66, 597-605.

10. Discher, D. E.; Janmey, P.; Wang, Y. L. Tissue Cells Feel and Respond to the Stiffness of Their Substrate. *Science* **2005**, 310, 1139-1143.

11. Nagase, K.; Kobayashi, J.; Okano, T. Temperature-Responsive Intelligent Interfaces for Biomolecular Separation and Cell Sheet Engineering. *J. R. Soc. Interface* **2009**, 6, S293-309.

12. Cole, M. A.; Voelcker, N. H.; Thissen, H.; Griesser, H. J. Stimuli-Responsive Interfaces and Systems for the Control of Protein-Surface and Cell-Surface Interactions. *Biomaterials* **2009**, 30 (9), 1827-1850.

13. Takezawa, T.; Mori, Y.; Yoshizato, K. Cell Culture on a Thermo-Responsive Polymer Surface. *Biotechnology (NY)* **1990**, 8, 854-856.

14. Schmidt, S.; Zeiser, M.; Hellweg, T.; Duschl, C.; Fery, A.; Möhwald, H. Adhesion and Mechanical Properties of PNIPAM Microgel Films and Their Potential Use as Switchable Cell Culture Substrates. *Adv. Func. Mater*. **2010**, 20, 3235-3243.

15. Wischerhoff, E.; Uhlig, K.; Lankenau, A.; Borner, H. G.; Laschewsky, A.; Duschl, C.; Lutz, J. F. Controlled Cell Adhesion on PEG-Based Switchable Surfaces. *Angew. Chem. Int. Ed. Engl*. **2008**, 47, 5666-5668.

16. Uhlig, K.; Boysen, B.; Lankenau, A.; Jaeger, M.; Wischerhoff, E.; Lutz, J. F.; Laschewsky, A.; Duschl, C. On the Influence of the Architecture of Poly(ethylene glycol)-Based Thermoresponsive Polymers on Cell Adhesion. *Biomicrofluidics* **2012**, 6, 24129.

17. Nakayama, M.; Okano, T.; Winnik, F. M. Poly(N-isopropylacrylamide)-Based Smart Surfaces for Cell Sheet Tissue Engineering. *Material Matters* **2010**, 5.3, 56-62.

18. da Silva, R. M.; Mano, J. F.; Reis, R. L. Smart Thermoresponsive Coatings and Surfaces for Tissue Engineering: Switching Cell-Material Boundaries. *Trends Biotechnol*. **2007**, 25, 577-583.

19. Fu, S. W.; Chien, H. W.; Tsai, W. B. Fabrication of Poly(N-isopropylacrylamide) Films Containing Submicrometer Grooves for Constructing Aligned Cell Sheets. *Langmuir* **2013**, 29, 14351-14355.

20. Tolan, M. X-ray Scattering from Soft-Matter Thin Films; Springer, 1999.

21. Zhong, Q.; Metwalli, E.; Rawolle, M.; Kaune, G.; Bivigou-Koumba, A. M.; Laschewsky, A.; Papadakis, C. M.; Cubitt, R.; Müller-Buschbaum, P. Structure and Thermal Response of Thin

Thermoresponsive Polystyrene-block-poly(methoxydiethylene glycol acrylate)-block-polystyrene Films. *Macromolecules*, **2013**, 46, 4069–4080.

22. Vidyasagar, A.; Majewski, J.; Toomey, R. Temperature Induced Volume-Phase Transitions in Surface-Tethered Poly(N-isopropylacrylamide) Networks. *Macromolecules* **2008**, 41, 919-924.

23. Vidyasagar, A.; Smith, H. L.; Majewski, J.; Toomey, R. G. Continuous and Discontinuous Volume-Phase Transitions in Surface-Tethered, Photo-Crosslinked Poly (N-isopropylacrylamide) Networks. *Soft Matter* **2009**, 5, 4733-4738.

24. Ashkar, R. Dynamical Theory Applications to Neutron Scattering from Periodic Nanostructures. Ph.D., Indiana University, 2012.

25. Ankner, J. F.; Tao, X.; Halbert, C. E.; Browning, J. F.; Michael Kilbey, S.; Swader, O. A.; Dadmun, M. S.; Kharlampieva, E.; Sukhishvili, S. A. The SNS Liquids Reflectometer. *Neutron News* **2008**, 19, 14-16.

26. Zhernenkov, M.; Fitzsimmons, M. R.; Chlistunoff, J.; Majewski, J.; Tudosa, I.; Fullerton, E. E. Electric-Field Modification of Magnetism in a Thin CoPd Film. *Phys. Rev. B* **2010**, 82, 024420.

27. Zhernenkov, M.; Jablin, M. S.; Misra, A.; Nastasi, M.; Wang, Y.; Demkowicz, M. J.; Baldwin, J. K.; Majewski, J. Trapping of Implanted He at Cu/Nb Interfaces Measured by Neutron Reflectometry. *Appl. Phys. Lett.* **2011**, 98, 241913.

28. Névot, L.; Croce, P. Caractérisation des Surfaces par Réflexion Rasante de Rayons X. Application à l'étude du Polissage de Quelques Verres Silicates. *Rev. Phys. Appl.* (Paris) **1980**, 15, 761-779.

29. Nelson, A. Co-Refinement of Multiple-Contrast Neutron/X-Ray Reflectivity Data Using MOTOFIT. *J. Appl. Cryst.* **2006**, 39, 273-276.

30. Ashkar, R.; Stonaha, P.; Washington, A. L.; Shah, V. R.; Fitzsimmons, M. R.; Maranville, B.; Majkrzak, C. F.; Lee, W. T.; Schaich, W. L.; Pynn, R. Dynamical Theory Calculations of Spin-Echo Resolved Grazing-Incidence Scattering from a Diffraction Grating. *J. Appl. Cryst.* **2010**, 43, 455-465.

31. Parratt, L. Surface Studies of Solids by Total Reflection of X-Rays. *Phys. Rev.* **1954**, 95, 359-369.

32. Milewska, A.; Szydlowski, J.; Rebelo, L. P. N. Viscosity and Ultrasonic Studies of Poly(N-isopropylacrylamide)–Water Solutions. *J. Polym. Sci. Pol. Phys.* **2003**, 41, 1219-1233.

33. LightSmyth Technologies http://www.lightsmyth.com/downloads/sem/SNS_C12_200xsec.jpg.

34. Wang,W.; Metwalli, E.; Perlich, J.; Papadakis, C. M.; Cubitt, R.; Müller-Buschbaum, P. Cyclic Switching of Water Storage in Thin Block Copolymer Films Containing Poly(N-isopropylacrylamide). *Macromolecules* **2009**, 42, 9041–9051

35. Jablin, M. S.; Dubey, M.; Zhernenkov, M.; Toomey, R.; Majewski, J. Influence of Lipid Membrane Rigidity on Properties of Supporting Polymer. *Biophys. J* **2011**, 101, 128-133.

36. Cole, M. A.; Voelcker, N. H.; Thissen, H.; Griesser, H. J. Stimuli-Responsive Interfaces and Systems for the Control of Protein–Surface and Cell–Surface Interactions. *Biomaterials* **2009**, 30, 1827-1850

37. Schmidt, S.; Motschmann, H.; Hellweg, T.; von Klitzing, R. Thermoresponsive Surfaces by Spin-Coating of PNIPAM-co-PAA Microgels: A Combined AFM and Ellipsometry Study. *Polymer* **2008**, 49, 749–756

38. Sun, J.; Ding, Y.; Lin, N. J.; Zhou, J.; Ro, H.; Soles, C. L.; Cicerone, M. T.; Lin-Gibson, S. Exploring Cellular Contact Guidance Using Gradient Nanogratings. *Biomacromolecules*, **2010**, 11, 3067–3072.
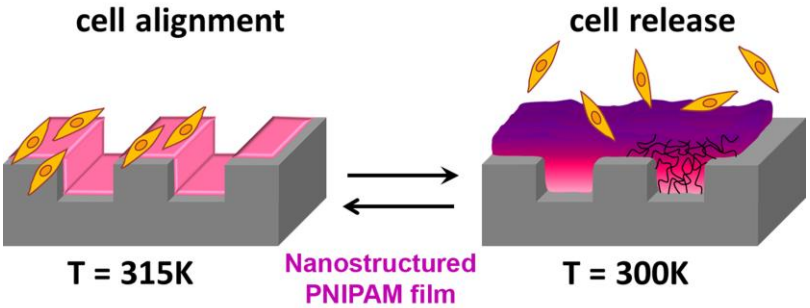
Table of Contents Graphic